Dynamics of Chua's Circuit

Amir Shapour Mohammadi
Princeton University, MAE541, Spring 2022

May 3, 2022

Contents

List of Figures

Abstract

The rich behavior of Chua's circuit has been known to manifest rich bifurcation phenomena and chaos via experiment and computer-assisted simulation. In this paper, the dynamics of Chua's circuit are examined and results from [1] are explored, ultimately demonstrating a rigorous proof of chaos. This paper will not be entirely rigorous with the formulation but will capture key features of the proof. The main objective is to reason the existence of a homoclinic orbit through the origin and use this to prove the existence of chaos using Shilnikov's Theorem.

Notation

Matrices and vectors are bold, $j = \sqrt{-1}$, $\triangleq$ denotes a definition. In addition, we will closely follow the labeling scheme in [1].

1 Introduction

We consider the set of electric circuits with time-dependent outputs and time-independent (DC) inputs, called autonomous circuits. A natural question to ask would then be which of the circuits in this large family can exhibit chaos. Although there are no necessary and sufficient conditions, an autonomous circuit exhibiting chaos must contain at least [2]

(C.1) one nonlinear element,
(C.2) one locally active resistor,
(C.3) three energy-storage elements (e.g. capacitors and inductors).

A nonlinear circuit element has a nonlinear relationship between the voltage and current across it. Without the nonlinear element, the dynamics are fairly simple and we have little hope of achieving chaos. A locally active resistor is a resistor which can amplify signals, producing (instead of consuming) power, for a range of voltage values applied across it. For our purposes it is sufficient to note that using Joule's Heating Law ($P = IV$), and assuming a nonlinear voltage-current relationship depicted in Figure (2), we see that P is positive in some regions, and negative in others. On the other hand, the voltage-current relationship of a typical resistor would be proportional to a straight line passing through the origin. The need for a power-producing element is evident as the energy in the circuit would otherwise dissipate away, preventing some complicated dynamics such as strange attractors.

At a first glance, these requirements are quite surprising since it implies that even if a circuit contains an arbitrary number of inductors and capacitors, and other elementary circuit elements, in an exceedingly complicated topology, it cannot exhibit chaos in the absence of a nonlinear and locally active resistor.

With these conditions in mind, we form Chua's circuit illustrated in Figure (1), consisting of one inductor with inductance L, one linear resistor with resistance R, two capacitors with capacitances C_1, C_2, and one nonlinear locally-active resistor N_R. Note that the linear resistor is in addition to the conditions of the above proposition. N_R satisfies **(C.1)** and **(C.2)** and the collection of inductor and capacitors satisfies **(C.3)**.

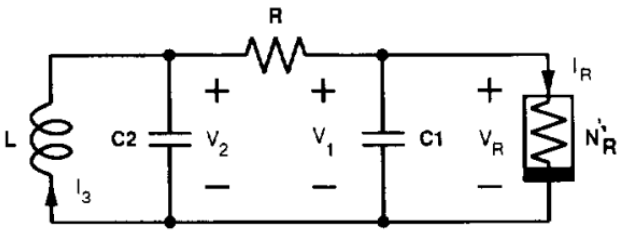

Figure 1: Chua's circuit [2].

There are numerous choices one could make for the topology of a circuit with these elements. There are also many redundancies in the circuits of other topologies, such as grouping R and N_R to be parallel one another, which simply reduces to adding a linear component to the voltage-current characteristic of N_R. Similarly, grouping C_1 and C_2 to be parallel to one another reduces the dynamics to that of one capacitor. There are many choices that we won't be able to justify apriori, such as the topology of the elementary circuit elements, but the importance of the existence of N_R will become abundantly clear.

2 Model Equations

Let v_1, v_2 be the voltage across C_1, C_2 respectively and let i_L be the current through L. Using Kirchhoff's Circuit Laws, we derive the following system of nonlinear, ordinary, first-order differential equations.

$$\begin{bmatrix} \dot{v}_1 \\ \dot{v}_2 \\ \dot{v}_3 \end{bmatrix} = \begin{bmatrix} \left((v_2 - v_1)\frac{1}{R} - g(v_1)\right)\frac{1}{C_1} \\ \left((v_1 - v_2)\frac{1}{R} + i_L\right)\frac{1}{C_2} \\ -\frac{1}{L}v_2 \end{bmatrix} \tag{1}$$

where $g(v_1)$ is a 3-segment piecewise-linear equation which is symmetric about the origin and describes the voltage characteristic of N_R. Note that this relationship incorporates a generalization of Ohm's Law ($V = IR$), which is only valid for linear resistors.

By rescaling the variables, and introducing parameters $\alpha, \beta \in \mathbb{R}$, $m_0 < 0, m_1 > 0$, we transform (1) into the equivalent third-order, dimension-less, autonomous, piecewise-linear differential equation:

$$\boxed{\dot{\mathbf{x}} \triangleq \begin{bmatrix} \dot{x} \\ \dot{y} \\ \dot{z} \end{bmatrix} = \begin{bmatrix} \alpha(y - h(x)) \\ x - y + z \\ -\beta y \end{bmatrix} \triangleq F(\mathbf{x})} \tag{2}$$

where

$$h(x) \triangleq m_1 x + \frac{1}{2}(m_0 - m_1)(|x + 1| - |x - 1|) \tag{3}$$

is a three-segment, odd-symmetric, piecewise-linear curve with critical points at $x = \pm 1$ (see Figure 2). We will now explore the dynamics of this system of equations, which we refer to as *Chua's equations*.

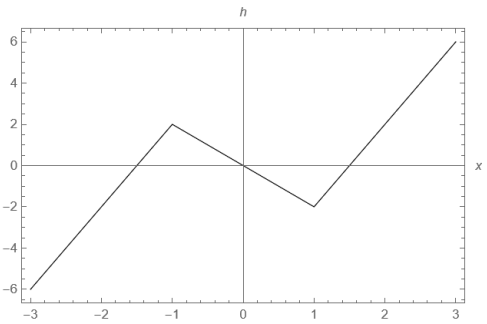

Figure 2: $h(x)$ with $m_0 = -1$, $m_1 = 4$.

3 Linear Dynamics

We start with exploring the linear dynamics of the Chua's equations and systems that are qualitatively similar, and cast them into normal form.

3.1 Linearized Chua's Equations

Due to the piecewise-linearity of Chua's equations, we will analyze each of the linear regions separately, using the following natural cover of $\mathbb{R}^3$

$$D_1 \triangleq \{\mathbf{x} : x \geq 1\},\ D_0 \triangleq \{\mathbf{x} : x \in [-1, 1]\},\ D_{-1} \triangleq \{\mathbf{x} : x \leq -1\}. \tag{4}$$

We also define the intersection of these regions which we will use later in defining the Poincare return map

$$U_1 \triangleq D_1 \cap D_0,\ U_{-1} \triangleq D_{-1} \cap D_0. \tag{5}$$

Note that in each region D_i, F is affine

$$dF(\mathbf{x}) = \begin{bmatrix} -\alpha(1+\gamma) & \alpha & 0 \\ 1 & -1 & 1 \\ 0 & -\beta & 0 \end{bmatrix} \tag{6}$$

where $\gamma = m_0 - 1$ if $\mathbf{x} \in D_0$, and $\gamma = m_1 - 1$ otherwise. This partition of $\mathbb{R}^3$ into disjoint regions where F is linear will become vital since we can gain better insight into the system as a whole by analyzing the dynamics in each set. F has equilibria $P^{\pm} \in D_{\pm 1} \setminus U_{\pm 1}$, $\mathbf{0} \in D_0$,

3.2 Class of Vector Fields $\mathfrak{L}$

The analysis explored in the remainder of this paper will apply to a large family of vector fields, and therefore, we will rigorously define this family, covering the essential features of Chua's equations that enables the complicated dynamics that we will demonstrate.

Let $\mathfrak{L}$ be a family of vector fields ξ satisfying the following properties.

(P.1): $\xi(-\mathbf{x}) = -\xi(\mathbf{x})$,
(P.2): There are two planes U_1, U_{-1} such that $\mathbf{x} \in U_1 \iff -\mathbf{x} \in U_{-1}$, and they partition

$\mathbb{R}^3$ into three regions D_i,
(P.3): $d\xi(\mathbf{x}) = \mathbf{M}_i \in \mathbb{R}^{3\times 3}$ for $\mathbf{x} \in D_i$ (i.e. ξ is affine in each region D_i),
(P.4): ξ has three equilibrium points, one in each D_i,
(P.5): For every i, $\mathbf{M}_i$ has a pair of complex conjugate eigenvalues,
(P.6): The eigenspaces of any of the equilibrium points are not parallel to U_1, U_2.

We label the complex eigenvalues of $\mathbf{M}_{\pm 1}$ by $\tilde{\sigma}_1 \pm j\tilde{\omega}_1$ and that of $\mathbf{M}_0$ by $\tilde{\sigma}_0 \pm j\tilde{\omega}_0$, and the real eigenvalues by $\tilde{\gamma}_1, \tilde{\gamma}_0$ respectively.

3.3 Partition of $\mathfrak{L}$

The objective is to quotient $\mathfrak{L}$ into equivalence classes of similar qualitative behavior, and analyze the dynamics of the equivalence class containing Chua's equations. If we were dealing with general vector fields, it would be natural to consider topological (C^0) equivalence. In fact, that is exactly what we will consider, but because we are working in the space of endomorphisms on $\mathbb{R}^3$, it is more accurate to use the definition of linear equivalence, which is generally a stronger condition, but coincides with topological equivalence in the case of linear maps.

Formally, $\xi, \tilde{\xi} \in \mathrm{End}(\mathbb{R}^n)$ are linearly equivalent if there exists $G \in \mathrm{Aut}(\mathbb{R}^n)$ such that $G \circ \xi = \nu(\tilde{\xi} \circ G)$ where $\nu \in \mathbb{R}$ is a constant scaling factor. An equivalent definition for vector fields in $\mathfrak{L}$, as is proved in [1], is that $\xi, \tilde{\xi} \in \mathfrak{L}$ have the same *normalized eigenvalue parameters*

$$\left\{ \frac{\tilde{\sigma}_0}{\tilde{\omega}_0}, \frac{\tilde{\gamma}_1}{\tilde{\omega}_1}, \frac{\tilde{\gamma}_0}{\tilde{\omega}_0}, \frac{\tilde{\sigma}_1}{\tilde{\omega}_1}, \frac{\tilde{\gamma}_0}{\tilde{\gamma}_1} \right\} \tag{7}$$

which we will use later to define an equivalence class of $\mathfrak{L}$ which contains Chua's equations.

3.4 Normal Form of Vector Fields in $\mathfrak{L}$

Due to symmetry, we will focus much of the analysis in the rest of this paper on only P^+ and U_+ (instead of also P^- and U_-) and $\mathbf{0}$. We begin by transforming each linear segment of $\xi \in \mathfrak{L}$ into Jordan form, and simultaneously simplify the expression for the planes $U_{\pm 1}$. It can be shown that due to **(P.5)**, there exist two maps $\Phi_0 : D_0 \to \mathbb{R}^3, \Phi_1 : D_1 \to \mathbb{R}^3$ such that

$$\Phi_0(\mathbf{0}) = \Phi_1(P^+) = \mathbf{0}, \tag{8}$$

$$V_0^{\pm 1} \triangleq \Phi_0(U_{\pm 1}) = \{\mathbf{x}' \in \mathbb{R}^3 : x' + z' = \pm 1\}, \tag{9}$$

$$V_1 \triangleq \Phi_1(U_1) = \{\mathbf{x}'' \in \mathbb{R}^3 : x'' + z'' = 1\}, \tag{10}$$

$$d(\Phi_0 \circ \xi \circ \Phi_0^{-1})(\mathbf{x}') = \frac{1}{\tilde{\omega_0}} \begin{bmatrix} \frac{\tilde{\sigma}_0}{\tilde{\omega}_0} & -1 & 0 \\ 1 & \sigma_0 & 0 \\ 0 & 0 & \frac{\tilde{\gamma}_0}{\tilde{\omega}_0} \end{bmatrix}, \; d(\Phi_1 \circ \xi \circ \Phi_1^{-1})(\mathbf{x}'') = \frac{1}{\tilde{\omega_1}} \begin{bmatrix} \frac{\tilde{\sigma}_1}{\tilde{\omega}_1} & -1 & 0 \\ 1 & \sigma_1 & 0 \\ 0 & 0 & \frac{\tilde{\gamma}_1}{\tilde{\omega}_1} \end{bmatrix}. \tag{11}$$

The particular Jordan forms above are not too important for our purposes, but are included for completion. The simplified forms of $U_{\pm 1}$ will greatly simplify our efforts to analyze the

dynamics of the system near the equilibria. Note that the coordinate systems defined by the maps Φ_0, Φ_1 are not necessarily the same (so they are labeled by $\mathbf{x}', \mathbf{x}''$ respectively). We will now define key points and planes (see Figure 3) which will be essential to defining the Poincare map in the next section

$$L_0 \triangleq U_1 \cap E^c(\mathbf{0}),\ L_1 \triangleq E^c(P^+) \cap U_1,\ L_2 \triangleq \{\mathbf{x} \in U_1 : \xi(\mathbf{x}) \parallel U_1\}, \tag{12}$$

$$A \triangleq L_0 \cap L_1,\ B \triangleq L_1 \cap L_2,\ E \triangleq L_0 \cap L_2,\ F \triangleq \{\mathbf{x} \in L_2 : \xi(\mathbf{x}) \parallel L_2\} \tag{13}$$

where $E^c(P^+), E^c(\mathbf{0})$ denote the two-dimensional center eigenspaces of P^+ and $\mathbf{0}$ respectively. Note that $L_i \subset U_1$ for each i. We claim without proof that $L_i \nparallel L_j$ for any $i \neq j$, and therefore A, B, E are well-defined, as well as all other quantities.

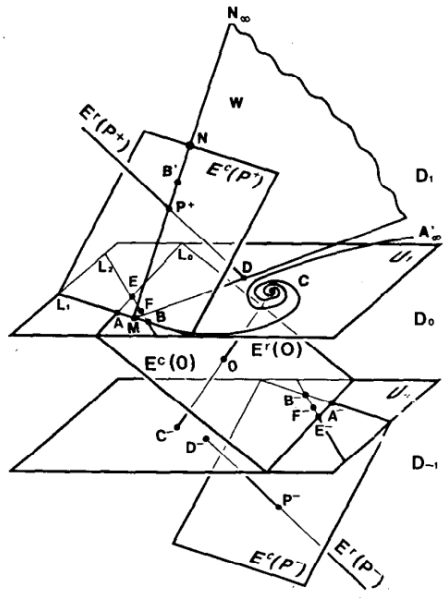

Figure 3: Dynamics of Chua's equations near equilibria and $U_{\pm 1}$ planes. Eigenspaces of equilibria, as well as key points and lines are depicted [1].

3.5 Double Scroll Family

We now shift our attention to a particular equivalence class of $\mathfrak{L}$ which we will show exhibits chaotic behavior, particularly a *double scroll strange attractor* demonstrated in Figure (5). We will prove and demonstrate that for a particular set of parameter values defined below, Chua's equations will exhibit this phenomena. We first define the *double scroll family*

$$\mathfrak{L}_{DS} \triangleq \left\{ \xi \in \mathfrak{L} : \frac{\tilde{\sigma}_0}{\tilde{\omega}_0}, \frac{\tilde{\gamma}_1}{\tilde{\omega}_1}, \frac{\tilde{\gamma}_0}{\tilde{\gamma}_1} < 0,\ \frac{\tilde{\gamma}_0}{\tilde{\omega}_0}, \frac{\tilde{\sigma}_1}{\tilde{\omega}_1} > 0 \right\}. \tag{14}$$

The motivation for this definition is to require that the corresponding eigenvalues of $P^{\pm 1}$ are a mirror image of that of $\mathbf{0}$ subject to a change of scale. With respect to Chua's equations, consider the parameter values

$$(\alpha, \beta, m_0, m_1) = (9.85, 14.3, -1/7, 2/7). \tag{15}$$

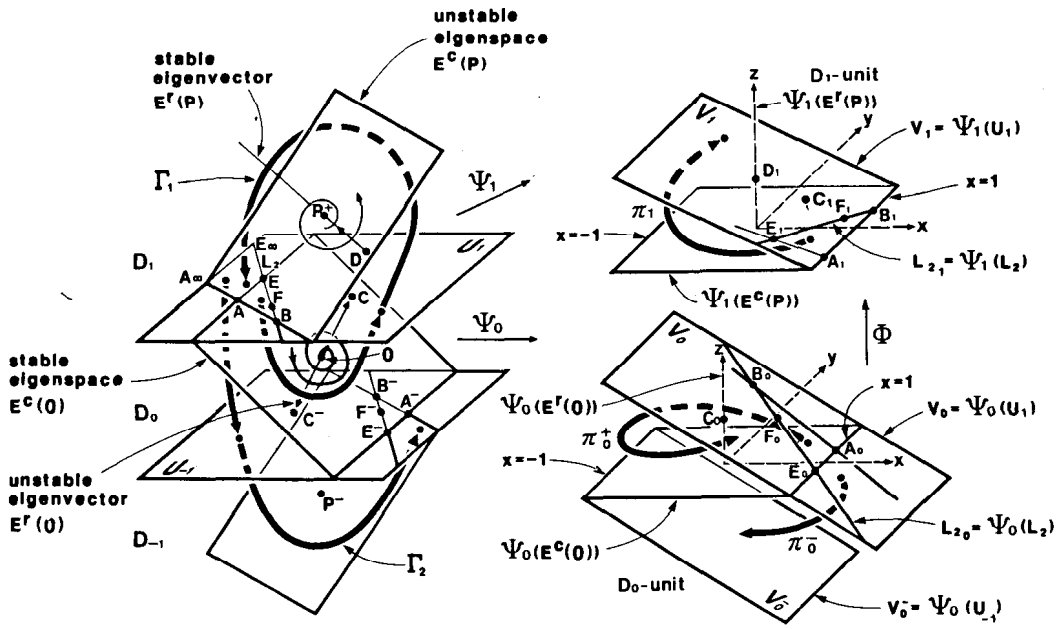

Figure 4: Original system, and transformation to normal form [1].

The eigenvalues of $dF(\mathbf{0})$ are calculated

$$-1.03197 \pm 2.66046j,\ 2.47109 \tag{16}$$

and that of $dF(P^+)$ are calculated

$$0.243308 \pm 3.04926j, -4.30009. \tag{17}$$

We see that $\tilde{\sigma}_0 = -1.03197, \tilde{\omega}_0 = 2.66046, \tilde{\gamma}_0 = 2.47109$, and $\tilde{\sigma}_1 = 0.243308, \tilde{\omega}_1 = 3.04926, \tilde{\gamma}_1 = -4.30009$, and therefore Chua's circuit is an element of $\mathfrak{L}_{DS}$ for the parameter values (15).

4 Poincare Half-Return Map

4.1 Normal Coordinate System for V_1

We begin by defining the points

$$A_1 \triangleq \Phi_1(A),\ B_1 \triangleq \Phi_1(B),\ E_1 \triangleq \Phi_1(E),\ F_1 \triangleq \Phi_1(F) \tag{18}$$

as simply the images of the points A, B, E under the map Φ_1. We parameterize V_1 using the map $y : (u, v) \in [0, \infty) \times [0, 1] \to V_1$

$$y(u, v) = u(vA_1 + (1 - v)E_1) + (1 - u)(vB_1 + (1 - v)F_1). \tag{19}$$

The importance of this coordinate system will become evident in the discussion of the Poincare map below.

4.2 Definition of Half-Return Map π_1

We also define the angular region

$$\angle A_1B_1E_1 \triangleq \{y(u,v) \in V_1 : (u,v) \in [0,\infty) \times [0,1]\}. \tag{20}$$

It turns out that any trajectory starting in this set has a downward ($-\hat{z}$ in the Φ_1 coordinate system) component to its velocity (see the right side of Figure 4). Note that $A_1 \cup E_1 = \{x = 1\} \cap \{z = 0\} \subset \Phi_1(E^c(\mathbf{0})), \angle A_1B_1E_1$, and therefore the above observation will hold equally well to it. By **(P.1)**, this implies that for $\{x = -1\} \cap \{z = 0\}$, any trajectory passing through this set has an upward component to its velocity, which will be used in the proof of the existence of a homoclinic orbit through the origin.

This downward behavior of $\angle A_1B_1E_1$ in conjunction with the upward behavior of $E^u(\mathbf{0})$ motivates us to define a *half-return* Poincare map from the region $\angle A_1B_1E_1$ into V_1. This helps us analyze how trajectories near the origin in the original system wind around the origin, and will help us understand the dynamics of homoclinic orbits in subsequent sections. The name half-return is motivated by the notion that the trajectory is half-complete in some sense since it must still traverse above the V_1 plane and loop back around, possibly intersecting V_1 for a second time.

We now define the half-return map $\pi_1 : \angle A_1B_1E_1 \subset V_1 \to V_1 = \Phi_1(U_1)$ such that $\pi_1(\mathbf{x}) = \phi_1^{-\tau}(\mathbf{x})$ where ϕ_1 is the flow map of the transformed system in $\Phi_1(D_1)$. T is naturally the time it takes for $\mathbf{x}$ to first return to V_1, or more rigorously,

$$\tau(\mathbf{x}) \triangleq \inf\{t > 0 : \phi_1^{-t}(\mathbf{x}) \in V_1\}. \tag{21}$$

We can compute π_1 explicitly using an algorithm discussed in [1]

$$\pi_1(y(u,v)) = e^{-\sigma_1\tau} \begin{bmatrix} \cos\tau & \sin\tau \\ -\sin\tau & \cos\tau \end{bmatrix} y(u,v). \tag{22}$$

We see that in the coordinate system (u,v) for V_1, π_1 is a logarithmic spiral, where the constant lines $u = const.$, $v = const.$ are mapped to spirals. Intuitively, the proximity to $E^c(\mathbf{0})$ twist the orbits into a spiral, while $E^u(\mathbf{0})$ accelerates them upward into V_1.

5 Shilnikov Chaos

5.1 Existence of Homoclinic Orbit through the Origin

We will now prove the existence of a homoclinic orbit through the origin $\mathbf{0}$, one of the conditions required to apply Shilnikov's Theorem. Let $C \triangleq U_1 \cap E^u(\mathbf{0})$, $\xi \in \mathfrak{L}_{DS}$, and assume the following conditions

(C.1): $(\pi_1^{-1} \circ \Psi_1)(C) \in \overline{A_1E_1}$,
(C.2) For any $\mathbf{x} \in \overline{A_0E_0}$, any trajectory starting at $\mathbf{x}$ does not intersect the line $\{x = -1\} \cap \{z = 0\} = -\overline{A_0E_0}$.

We start by considering the trajectory Γ_0 (in the original coordinate system) that passes through $\mathbf{0}$ and is tangent to $E^u(\mathbf{0})$ such that it intersects U_1 at C. Note that $\Phi_1(C) \in \Phi_1(U_1) = V_1$ (since $C \in U_1$). By assumption **(C.2)**, we have that $\pi_1^{-1}(\Phi_1(C)) \in \overline{A_1E_1} = \Phi_1(\overline{AE})$. Taking an inverse, we have that $C_1 \triangleq (\Phi_1^{-1} \circ \pi_1^{-1} \circ \Phi_1)(C) \in \overline{AE}$, and therefore, the trajectory Γ_C through C must intersect the point $C_1 \in \overline{AE}$. Since $\overline{AE} \subset E^c(\mathbf{0})$, and the trajectory Γ_{C_1} through C_1 does not intersect U_{-1} (by **(C.2)**), it does not move upwards (or downwards). Therefore, it must remain on $E^c(\mathbf{0})$ indefinitely, and therefore converge to $\mathbf{0}$ as $t \to \infty$. Therefore, the combined trajectory $\Gamma = \Gamma_0 \cup \Gamma_C \cup \Gamma_{C_1}$ converges to $\mathbf{0}$ as $t \to -\infty$ (by construction of Γ_0), and converges to $\mathbf{0}$ as $t \to \infty$ by the previous sentence. Hence, we have proved the existence of a homoclinic orbit Γ through the origin.

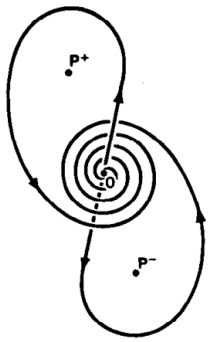

Figure 5: Pair of odd-symmetric, Shilnikov-type homoclinic orbits passing through the origin [1].

5.2 Applying Shilnikov's Theorem

We first recall Shilnikov's Theorem [8], which we will then use to show the existence of chaos near the origin of Chua's equations.

Suppose we have a third-order autonomous system such that $\mathbf{0}$ is an equilibrium point with eigenvalues $\sigma \pm j\omega$, γ where $\sigma < 0, \omega \neq 0, |\sigma| < \gamma$, and $\gamma > 0$. If there exists a homoclinic orbit through $\mathbf{0}$ then the system can be perturbed to contain a countable set of horseshoes, and therefore exhibits chaos.

In the previous section (5.1), we proved that it is sufficient to show **(C.1)**, **(C.2)** in order to prove the existence of a homoclinic orbit through $\mathbf{0}$. We will not prove this for Chua's equations as it is a tedious computation but refer the interested reader to [1]. We will now show that the constraints on the eigenvalues of dF are satisfied by the set of parameter values (15). Assuming (15), recall the eigenvalues of $dF(\mathbf{0})$

$$-1.03197 \pm 2.66046j,\ 2.47109 \tag{23}$$

In the notation of Shilnikov's Theorem, we have $\sigma = -1.03197 < 0, \omega = 2.66046 \neq 0, \gamma = 2.47109 > 0, |\sigma| = 1.03197 < 2.47109 = \gamma$. Hence, applying Shilnikov's Theorem, this system exhibits chaos (see Figures 5, 6).

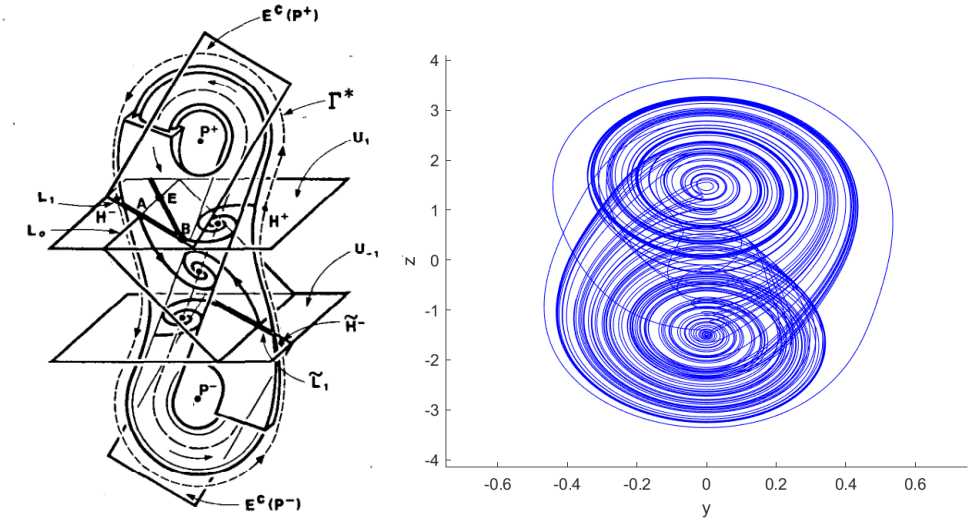

Figure 6: Double scroll strange attractor. (a) Illustrative description of orbits [1]. (b) Simulation with the parameter values (15) and initial coordinates $\mathbf{x}_0 = (0.2, 0, -1.4)$.

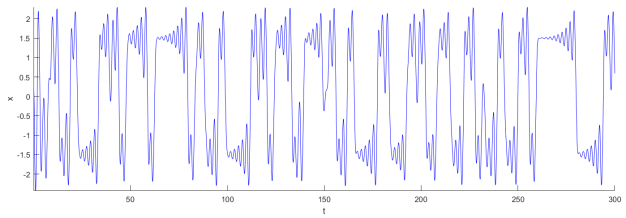

(a) x(t)

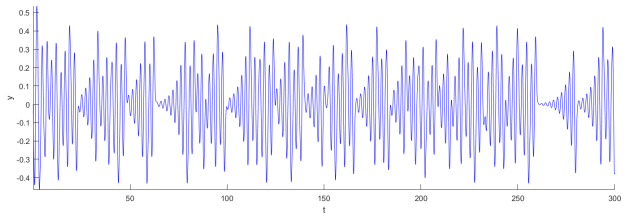

(b) y(t)

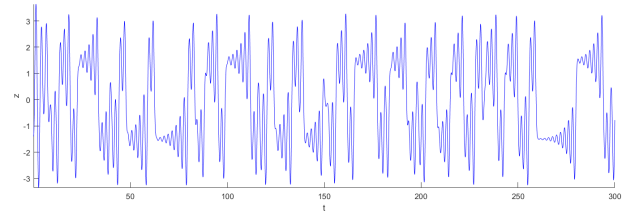

(c) z(t)

Figure 7: Time-series plots of chaotic dynamics near the origin for parameter values (15) and initial coordinates $\mathbf{x}_0 = (0.2, 0, -1.4)$

6 Conclusion

In this paper, we have examined the dynamics of a large class of vector fields $\mathfrak{L}_{DS}$, which includes Chua's equations. We motivated the pursuit of Chua's circuit for complicated dynamics, and significantly simplified the system by performing multiple change of coordinates. We then defined the half-return map which was used in proving the existence of a homoclinic orbit through the origin. It was proved that Chua's circuit exhibits chaos in the sense of Shilnikov's Theorem for (but not limited to) a particular set of parameter values. We simulated the system, with the aforementioned parameter values, and confirmed the existence of a double scroll strange attractor. We tried to encapsulate as much of the proof of chaos as possible, but to better understand the argument, the steps which we skipped over, such as that Chua's circuit satisfies **(C.1)** and **(C.2)** should be further examined in [1].

References

[1] Chua, L., et al. “The Double Scroll Family.” IEEE Transactions on Circuits and Systems, vol. 33, no. 11, 1986, pp. 1072–1118., https://doi.org/10.1109/tcs.1986.1085869.

[2] Kennedy, M.P. “Three Steps to Chaos. I. Evolution.” IEEE Transactions on Circuits and Systems I: Fundamental Theory and Applications, vol. 40, no. 10, 1993, pp. 640–656., https://doi.org/10.1109/81.246140.

[3] Fortuna, Luigi, et al. Chua’s Circuit Implementations Yesterday, Today and Tomorrow. World Scientific, 2009.

[4] Li, Qingdu, et al. “On Hidden Twin Attractors and Bifurcation in the Chua’s Circuit.” Nonlinear Dynamics, vol. 77, no. 1-2, 2014, pp. 255–266., https://doi.org/10.1007/s11071-014-1290-8.

[5] Li, Junze, et al. “Zero-Hopf Bifurcation and Hopf Bifurcation for Smooth Chua’s System.” Advances in Difference Equations, vol. 2018, no. 1, 2018, https://doi.org/10.1186/s13662-018-1597-8.

[6] Medrano-T., R. O., et al. “Shilnikov Homoclinic Orbit Bifurcations in the Chua’s Circuit.” Chaos: An Interdisciplinary Journal of Nonlinear Science, vol. 16, no. 4, 2006, p. 043119., https://doi.org/10.1063/1.2401060.

[7] Kahan, Sandra, and Anibal C. Sicardi-Schifino. “Homoclinic Bifurcations in Chua’s Circuit.” Physica A: Statistical Mechanics and Its Applications, vol. 262, no. 1-2, 1999, pp. 144–152., https://doi.org/10.1016/s0378-4371(98)00389-6.

[8] Guckenheimer, John, and Philip Holmes. “Nonlinear Oscillations, Dynamical Systems, and Bifurcations of Vector Fields.” Applied Mathematical Sciences, 1983, https://doi.org/10.1007/978-1-4612-1140-2.